International Journal of Thermophysics, Vol. 23, No. 5, September 2002 (© 2002)

Thermophysical Properties of Zirconium Alloy E110 (Zr-0.01Nb) after Oxidation in Air Atmosphere[1]

I. I. Petrova,[2, 3] B. N. Samsonov,[2] V. E. Peletsky,[2] A. V. Nikulina,[4] N. B. Sokolov,[4] and L. N. Andreeva-Andrievskaya[4]

The subsecond resistive pulse heating technique has been used to study the temperature dependence of the heat capacity and spectral emissivity (for the wavelength of 0.65 μm) of the zirconium alloy E110 (Zr-0.01Nb) after oxidation in air atmosphere. The tubular samples were oxidized at multiple pulse heating cycles up to different maximum temperatures (1200, 1300, 1400, 1500, and 1600 K) and subsequent cooling. It is shown that the thermophysical properties of the oxidized samples depend on the maximum temperature of oxidation.

KEY WORDS: heat capacity; oxidation; spectral emissivity; subsecond resistive pulse heating; zirconium alloy.

1. INTRODUCTION

Zirconium alloys are used in nuclear power engineering as a cladding for the fuel elements and other parts of nuclear reactors. Reliable data on thermophysical properties of these alloys are necessary to predict the behavior of the fuel elements both at normal operation and at design basis accidents. At the accident conditions, when the reactor may lose coolant, the destructive influence of high temperatures and oxidized ambient atmosphere have an effect on the cladding.

The oxidized cladding is a complex system, which consists of the oxygen solid solution in the alloy with variable concentration of oxygen at

[1] Paper presented at the Sixth International Workshop on Subsecond Thermophysics, September 26–28, 2001, Leoben, Austria.

[2] Institute for High Energy Densities, Associated Institute for High Temperatures, Izhorskaya 13/19, 127412 Moscow, Russia.

[3] To whom correspondence should be addressed. E-mail: petrova_i@hotbox.ru

[4] Federal State Unitary Enterprise, A.A. Bochvar All-Russia Research Institute of Inorganic Materials, VNIINM, Rogova 5a, 123060 Moscow, Russia.

0195-928X/02/0900-1347/0 © 2002 Plenum Publishing Corporation

the tube cross section and oxide films on both surfaces. The thickness and phase structure of the films depend on the temperature and heating time. Thermophysical property calculations for this system are very difficult. In addition, the zirconium alloy and its oxide have property anomalies at the temperature ranges of the phase transitions. Thus, the experimental study of thermophysical properties of the oxidized cladding is the subject of this paper.

Following our previous study of another zirconium alloy [1], the oxidized environment has a great influence on thermophysical properties, especially at the phase transition areas. The measurements [1] have been made in air atmosphere. In the present work the experiments were performed in inert atmosphere (argon) up to the melting temperature. All samples were previously oxidized.

2. SAMPLES

All of the samples were made from commercial tubes for nuclear fuel elements. The length of the studied tubular samples was ~ 75 mm; their external diameter was ~ 9.1 mm; and their internal diameter was ~ 7.7 mm. The distance between two probes in the central part of the sample, where the voltage drop was measured, was equal to 10 mm. The blackbody model for the measurement of the true temperature was made with a rectangular slit, 20 mm long and 1.5 mm wide. All dimensions above are for the unoxidized samples. The mass and dimension deviations of the samples after oxidation were taken into account in further calculations. Two high-speed photoelectric pyrometers (both with a wavelength $\lambda = 0.65$ μm) measured synchronously the radiance and true temperatures of the sample during the experiment. All quantities (the electrical current I, the voltage drop U, true temperature T_{tr}, and brightness (radiance) temperature T_{br}) were measured as a function of time τ using an A/D-converter with a rate of 1000 samples/s.

The heat capacity C_{p} and the spectral emissivity ε_λ ($\lambda = 0.65$ μm) were calculated with the following expressions:

$$C_{\text{p}} = \frac{UI - q_r}{m\left(\frac{dT}{d\tau}\right)_h} \tag{1}$$

$$\ln \varepsilon_\lambda = \frac{c_2}{\lambda}\left(\frac{1}{T_{\text{tr}}} - \frac{1}{T_{\text{br}}}\right) \tag{2}$$

In these expressions m is the mass of the central section of the sample, $C_2 = 1.4388 \cdot 10^{-2}$ m·K is the second constant in Planck's law, $(dT/d\tau)_h$ is the heating rate, q_r is a correction for the radiation heat loss.

The experimental technique and the principle of measurement are described in Refs. 1 and 2.

The samples were oxidized in air atmosphere at normal pressure with multiple cycles of pulse resistive heating and subsequent cooling. The maximum heating temperatures T_{ox} were equal to 1200, 1300, 1400, 1500, and 1600 K for the different samples accordingly. At the end of the cooling stage the temperature was about 900 K for all samples (the lower limit of the pyrometer). The number of heating and cooling cycles was 50 for each sample. The total time of these cycles was about 20 min. The heating was switched off by the programmed computer control due to the signal from the D/A-converter after reaching the selected maximum temperature by the sample.

For each of the chosen temperature regimes two samples were oxidized: the first for experimental measurements and the other for a metallographic study. As may be seen from Fig. 1, with an increase of the highest temperature of oxidation T_{ox}, the oxide film thickness δ increases. The increase of the specific mass of the working section $\Delta m/F$ was observed also. These characteristics are given in Table I. X-ray analysis, which was performed on the sample, oxidized at $T_{ox} = 1600$ K, showed that the greater part of the wall cross section of the tubular sample was the oxygen solid solution in α-zirconium with variable concentration along the cross section from 0 at.% at the middle to 30 at% at the border with the oxide layer. The oxide film consists of two phases which are the zirconium oxide and the oxygen solid solution in α-zirconium with a maximum concentration of about 30 at%. The ratio of these components along the film cross section is variable. The main component of this film in the near-surface region is the zirconium oxide. With the increase of T_{ox}, the oxide on the sample surface is transformed from dark (non-stoichiometric) for $T_{ox} = 1200$ K to white (stoichiometric) for $T_{ox} = 1600$ K. The results of microhardness measurements along the cross section of the oxidized samples are correlated with X-ray analysis and presented in Fig. 2. The measurements of microhardness was carried out by apparatus PMT-3 with a load of 50 g. The uncertainty of these measurements was 6 $kg \cdot mm^{-2}$.

3. RESULTS AND DISCUSSION

3.1. Thermograms

The experiments with oxidized samples of Zr-0.01Nb alloy were performed in argon atmosphere at a low pressure ($P = 0.11$ MPa). The heating thermograms for the oxidized samples at the different highest temperatures of oxidation T_{ox}, equal to 1300, 1400, 1500, and 1600 K (curves 2 to 5) and

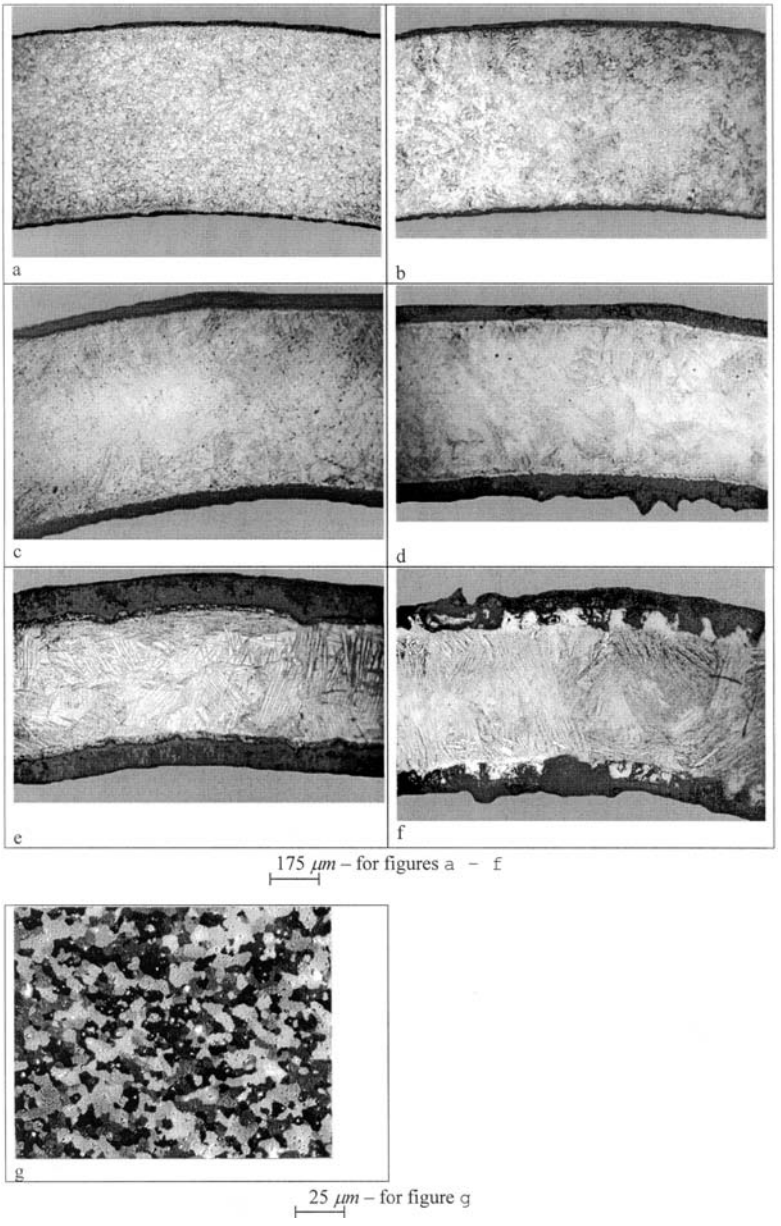

Fig. 1. Photomicrographs of the cross sections of the samples, oxidized at different temperatures T_{ox}: (a) 1200 K; (b) 1300 K; (c) 1400 K; (d) 1500 K; (e) 1600 K; (f) oxidized at 1500 K and heated to melting; (g) non-oxidized sample.

Table I. Characteristics of Test Samples. (T_{ox}, the maximum heating temperature at oxidation; $\Delta m/F$, specific mass of the working section; δ, the oxide film thickness; T_α and T_β, the temperatures of the beginning and the end of the α-β transition; ΔT_δ, the film temperature drops; $C_{\alpha\text{-}\beta}$, the oxygen concentration in the solid solution in the α-β transition area; T_S, the solidus temperature; $C_{S\text{-}L}$, the oxygen concentration in the solid solution in the melting area.)

T_{ox} (K)	$[\Delta m/F]\times 10^2$ (g·m^{-2})	δ (mm)	T_β (K)	T_α (K)	ΔT_δ (K)	$C_{\alpha\text{-}\beta}$ (at%)	T_S (K)	$C_{S\text{-}L}$ (at%)
1200	0.0523	0.014	1186	1137	15	0.7	2173	8.2
1300	0.1481	0.021	1207	1151	30	1.0	2192	9.2
1400	0.1978	0.043	1272	1168	58	1.8	2198	9.8
1500	0.3832	0.071	1296	1178	85	2.2	2213	10.2
1600	0.6160	0.114	1503	1223	113	4.4	2217	10.5
non-oxid.	–	–	1195	1125	70	–	2100	–

for the non-oxidized sample (curve 1) are presented in Fig. 3. The curve for the non-oxidized sample is almost the same as for the sample oxidized at 1200 K. The α-β phase transition of the oxidized samples is not clearly in the thermograms because there is the distribution of the oxygen content along the cross section. During heating the α-β transition begins at the center of cross section, where the oxygen concentration is low, and finishes at the boundaries with oxide films, where the concentration of dissolved oxygen is high. Therefore, when the α-β phase transition near these

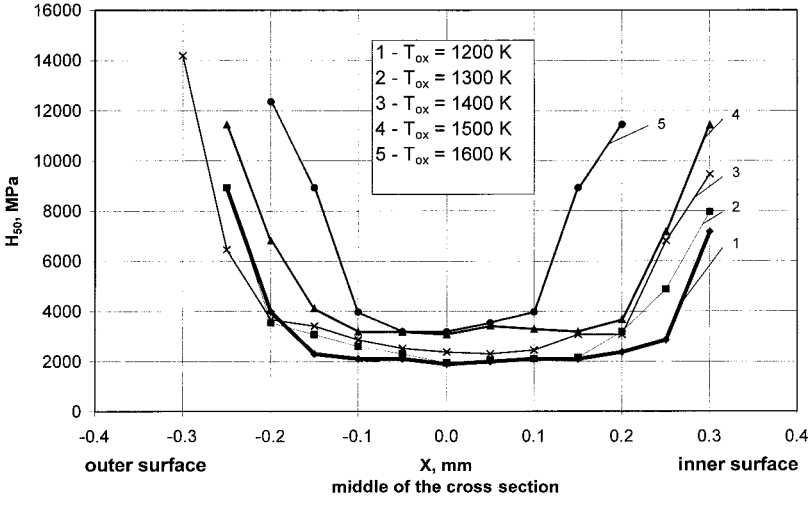

Fig. 2. Distribution of the microhardness H_{50} along the cross section of the tube wall, oxidized at different temperatures T_{ox}.

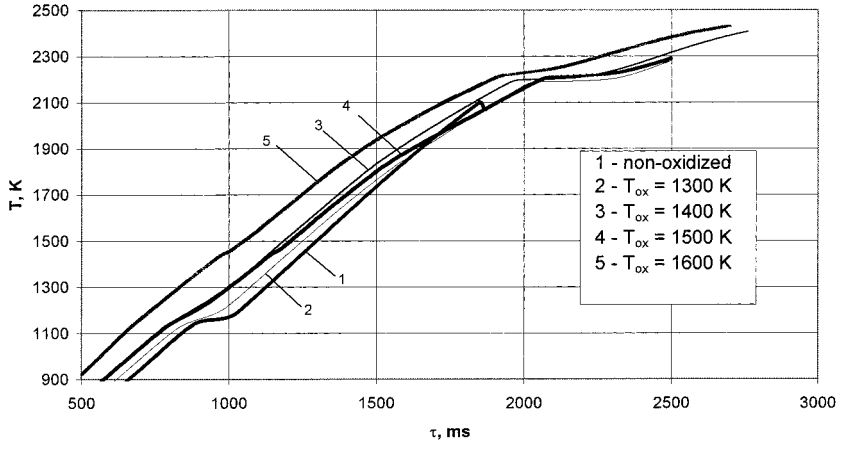

Fig. 3. Heating thermograms of the samples oxidized at different temperatures T_{ox}, and the non-oxidized sample.

boundaries finishes, the temperature of the central part of the cross section is higher than the local temperature of the α-β transition end.

The thermograms are given without correction for the temperature distribution along the cross section. This distribution is difficult to calculate as it is caused by different values for resistivity, as a fact of the difference in the oxygen concentration along the cross section. The temperature difference between the middle of the wall cross section and the surface had been evaluated for the sample oxidized at $T_{ox} = 1200$ K. For this regime the temperature of the α-β transition (T_α) must be equal to T_α for the non-oxidized sample, as their microhardness is equal. It was assumed that the temperature drops for the other regimes of oxidation were directly proportional to the oxide film thickness, as the maximum variations of the electrical resistivity take place in the oxide film. The evaluated data on the film temperature drops ΔT_δ and the temperatures of the beginning T_α and the end T_β of the α-β transitions are presented in Table I. These temperatures were determined according to the results for the electrical resistivity as a function of temperature $\rho = f(T)$ for each temperature regime of oxidation at the extremum points: $\rho_{max,\alpha}$—the maximum value of resistivity in the α-phase, and $\rho_{min,\beta}$ is the minimum value of resistivity in the β-phase.

At a temperature of about 1800 K a decrease of the heating rate was observed (Fig. 3). We suppose that an oxide film destruction and a formation of cracks take place. This may lead to an increase of thermal resistance between the metal and the oxide film. The photomicrographs of the samples cross section, which were heated up to melting, show the cracks in

the oxide film and its destruction. These cracks have not seen on the photomicrograph of the samples, heated to the temperatures less than 1800 K.

Unfortunately, we have no data on the oxygen concentration distribution along the cross section of the oxidized samples. Evaluation of the concentration in the solid solution parts of the samples for every oxidizing condition has been made using the measured phase transition temperatures (α-β and melting) and the Zr-O phase diagram [3]. As the microhardness is linearly dependent on concentration [4], we can judge the distribution of the concentration along the cross section using the results of microhardness measurements. The microhardness in the middle of the cross section is a minimum and shows very little change with an increase of the oxidation temperature, as can be seen from Fig. 2. For the samples oxidized at 1200 and 1300 K, the microhardnesses in the middle of the cross section are almost the same as for the non-oxidized sample, i.e., $H_{50} = 2000$ MPa [5]. The microhardness sharply increases near the surface. Evaluations of the oxygen concentration show that in the melting temperature region the oxygen concentration in the solid solution is higher than in the α-β transition region. The increase of the oxygen concentration in the solid solution corresponds with the higher solidus temperature T_S for each regime of oxidation.

The mean value of the oxygen concentration in the solid solution in the melting area $C_{S\text{-}L}$ changes from 8 to 10 at% for oxidizing temperatures from 1200 to 1600 K. In the temperature range of the α-β transition, the oxygen concentration in the solid solution $C_{\alpha\text{-}\beta}$ is smaller. The minimum concentration in the middle of the wall cross section was estimated, and it changes from 0 to 1 at% for oxidizing conditions from 1200 to 1600 K. The maximum concentration, evaluated on the temperature end of the α-β transition, changes within 0.7 to 4.4 at% for the same conditions. As it can be seen from the thermograms (Fig. 3), the end of melting is not sharply marked. It is associated with the oxygen concentration increase in the solid solution near the oxide film border. The evaluated concentrations and the measured solidus temperatures T_S for all conditions are presented in Table I.

3.2. Heat Capacity

The temperature dependences of the heat capacity $C_p = f(T)$ obtained for the oxidized samples of the E110 alloy are presented in Fig. 4. Curves 2 to 5 are for the samples oxidized at 1300 to 1600 K and curve 1 is for the non-oxidized sample. It can be seen that the heat capacity of the non-oxidized sample is almost the same as for the sample oxidized at 1200 K. There are three groups of abnormal peaks on the heat capacity curves. The

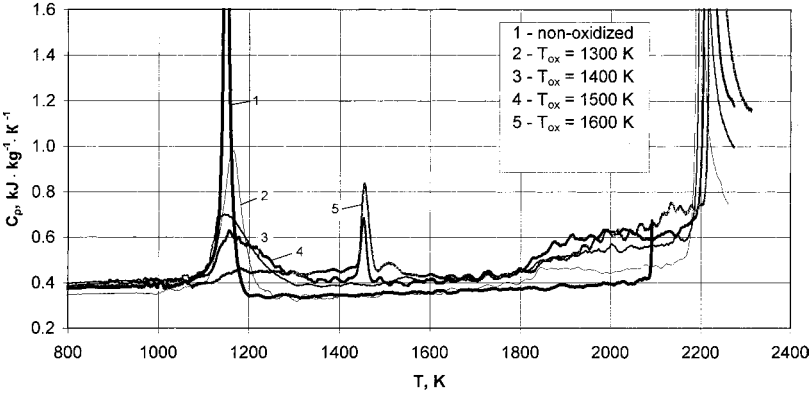

Fig. 4. Temperature dependences of the heat capacity C_p of the samples oxidized at different temperatures T_{ox} and the non-oxidized sample.

first group of peaks is caused by the α-β phase transition in the oxygen solid solution. In this group the maximum heat capacity peak is on curve 1. With an increase of the oxidation temperature the first heat capacity peak becomes lower and wider. This peak practically degenerates at $T_{ox} =$ 1600 K (curve 5). The reason for this heat capacity behavior is the change of the solid solution oxygen concentration. Just like the microhardness changes with an increase of the oxidizing temperature, the oxygen concentration changes slightly in the middle of the wall, but it sharply increases near the oxide film border. Therefore, the heat capacity peak expansion takes place in the direction of the β-phase, because of the increase of the temperature of the phase transition end.

The second peak on the heat capacity curves at $T \cong 1450$ K appears only for oxidized samples at 1500 and 1600 K (curves 4, 5). This is the zirconium oxide transition from monoclinic to tetragonal structure in the oxide film according to the phase diagram of Zr-O (Fig. 5) from Ref. 3. This second peak amplitude becomes higher as the film thickness increases. When the oxide film is thin ($T_{ox} = 1200$, 1300, and 1400 K), this peak on the heat capacity curves is not observed.

The observed increase of the heat capacity at temperatures above $T = 1800$ K may be related (as mentioned above) with the formation of cracks in the oxide films due to high thermal stress. The cracks may increase the thermal resistance of the film, and the film temperature, which is measured by the pyrometer, is lower than the metal temperature. The higher the oxidation temperature, the thicker the oxide film and the greater the observed heat capacity increase at a temperature near 1800 K.

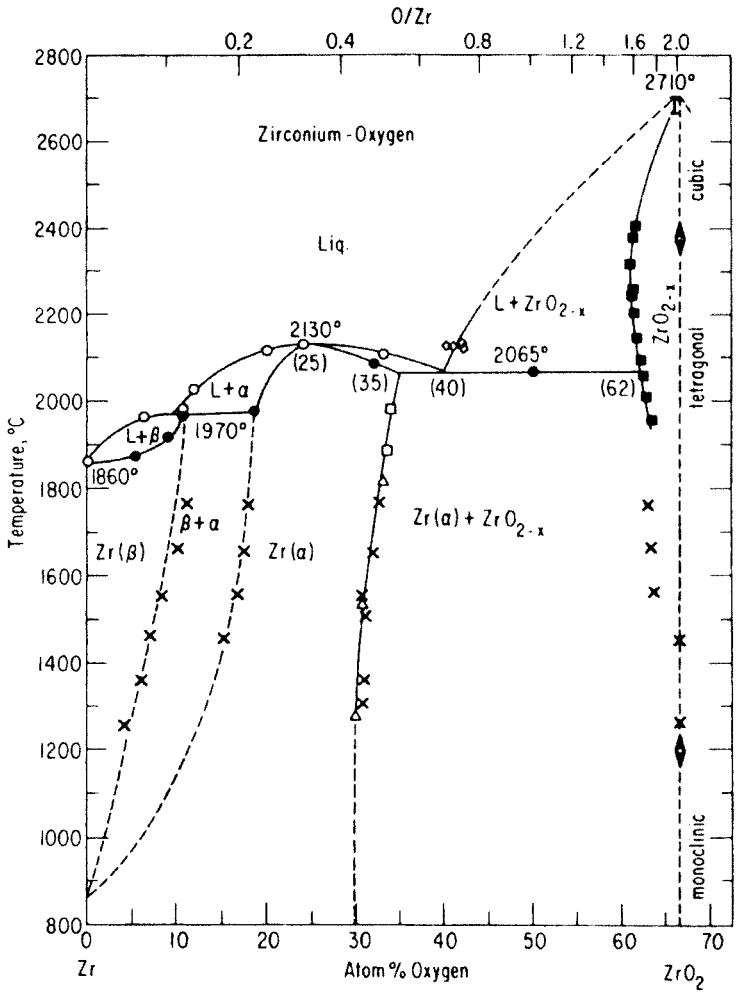

Fig. 5. Phase diagram Zr-O [3].

The third peak on the heat capacity curve is related to the melting of the sample. With an increase of the oxidation temperature it expands into the higher temperature area. It may be explained, as well, by an increase of the oxygen concentration in the solid solution near the oxide film border. The concentration does not increase significantly at the middle of the wall, so the left edges of the third peak do not shift significantly for different oxidizing conditions.

3.3. Spectral Emissivity ($\lambda = 0.65$ μm)

The temperature dependences of the spectral emissivity ε_λ ($\lambda = 0.65$ μm) for different E110 alloy samples are presented in Fig. 6. Curves 2 to 6 present results for samples oxidized at 1200 to 1600 K and curve 1 is for the non-oxidized sample. Mainly the outside thin layer of the oxide film determines the emissivity of the oxidized samples. The structure and the color of the film depend on the oxidizing temperature. The sample, which was oxidized at 1200 K, has the darkest surface (non-stoichiometric oxide) and its emissivity is the highest. The surface of the samples oxidized at 1300 and 1400 K becomes brighter. It is entirely white (stochiometric oxide) at $T_{ox} = 1500$ and 1600 K. The X-ray phase-structure study has shown that 98% of these sample surfaces consists of ZrO_2. It is necessary to note that with the increase of the oxidation temperature the surface of the samples becomes rough and knobby. Splits appear, and the white layer partially disappears and the dark underlayer of non-stoichiometric oxide becomes visible. Probably, just this dark underlayer makes the emissivity higher for the samples, oxidized at 1400 and 1500 K in comparison with the sample oxidized at 1300 K. The samples, oxidized at 1600 K, has the dense and white oxide film. So the spectral emissivity of these samples is lower than the emissivity of the other samples. Therefore, the expected temperature dependence $\varepsilon_\lambda = f(T_{ox})$ was not observed, as can be seen from Fig. 6. Thus, the thickness of the outside semitransparent white layer of the stoichiometric oxide does not completely determine the emissivity. The deeper layers of the non-stoichiometric oxide have the main influence on ε_λ. The

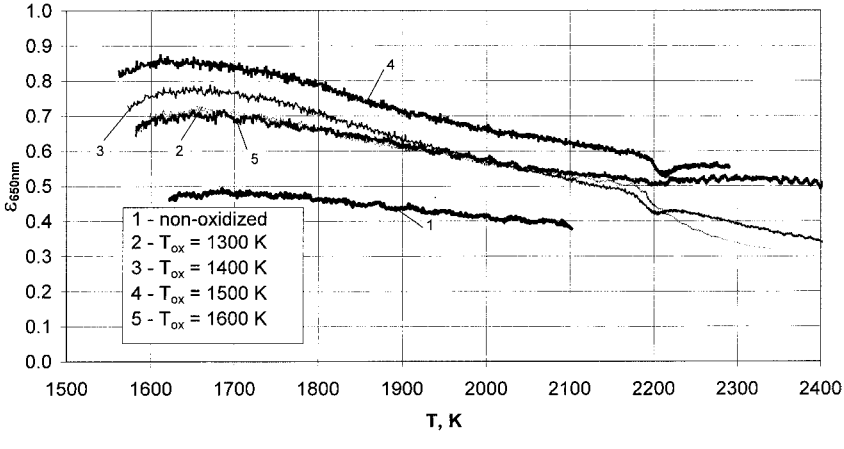

Fig. 6. Temperature dependences of the spectral emissivity ε ($\lambda = 0.65$ μm) of the samples oxidized at different temperatures T_{ox} and the non-oxidized sample.

character of the dependence $\varepsilon_\lambda = f(T)$ is similar for all studied samples: ε_λ decreases with increasing temperature; there are small negative peaks in the melting region, and than ε_λ decreases when the main internal part of the samples is molten.

3.4. Estimation of Errors

The total (systematic + random) uncertainties in the determination of the heat capacity and the spectral emissivity over the complete temperature range excluding the region of the α-β phase transition do not exceed 4.0 and 4.5%, respectively. The total uncertainties for the heat capacity in the region of the abnormal peaks are much higher and can reach 10 to 12%.

4. CONCLUSION

The temperature dependences of the heat capacity and the spectral emissivity of E110 zirconium alloy oxidized at various temperatures have been studied. The test samples were previously oxidized in air atmosphere in the course of 50 cycles of pulse heating up to various temperatures: 1200, 1300, 1400, 1500, and 1600 K. The oxidized samples are a complex system. It consists for the main part of zirconium-oxygen solid solution with variable concentration along the cross section and the outside layers of two-phase oxide films. The film consists of the zirconium oxide and oxygen saturated solid solution of the α-zirconium. Some peculiarities of the temperature dependence on the thermophysical properties for oxidized alloys are revealed. With an increase of the highest temperature of oxidation from 1200 to 1600 K, the following results are observed:

(i) a decrease of the first peak amplitude (α-β phase transition), the appearance of a second peak at $T \cong 1450$ K (structural transition in the zirconium oxide), and a shift of the third peak (melting) to higher temperatures on the $C_p = f(T)$ curves;

(ii) an observed increase of the heat capacity at $T \cong 1800$ K which may be related to the oxide film destruction and appearance of cracks;

(iii) an increase of the spectral emissivity (in comparison with the non-oxidized alloy sample) over the complete measured temperature range due to the dark (non-stoichiometric oxide) underlayer. The thickness of the white outside layer of the oxide does not have a major influence on the value of ε_λ. The discrepancy of the $\varepsilon_\lambda = f(T)$ curves for the samples oxidized at different maximum temperatures is related to the structure and composition of the outer film layers.

REFERENCES

1. I. I. Petrova, V. E. Peletsky, B. N. Samsonov, A. V. Nikulina, N. B. Sokolov, and L. N. Andreeva-Andrievskaya, (http://www.symp14.nist.gov/PDF/SUB02PET.PDF), 2000.
2. I. I. Petrova, V. E. Peletsky, and B. N. Samsonov, *Int. J. Thermophys.* **20**:1117 (1999).
3. R. J. Ackermann, S. P. Garg, and E. G. Rauh, *J. Amer. Ceramic Soc.* **60**:341 (1977).
4. I. I. Kornilov and V. V. Glasova, in *Vzaimodeystvie tugoplavkih metallov perehodnyh grupp s kislorodom* (Nauka, Moskva, 1967), p. 80.
5. A. C. Zaimovsky, A. V. Nikulina, and N. G. Reshetnikov, in *Zirconievye splavy v yadernoy energetike* (Energoatomizdat, Moskva, 1994), p. 256.